# Probing copper-boron interactions in the $Cu_2B_8^-$ bimetallic cluster

Cite as: J. Vac. Sci. Technol. A **40**, 042201 (2022); https://doi.org/10.1116/6.0001833 Submitted: 25 February 2022 • Accepted: 10 May 2022 • Published Online: 27 May 2022

Maksim Kulichenko, Wei-Jia Chen, Hyun Wook Choi, et al.













## Probing copper-boron interactions in the Cu<sub>2</sub>B<sub>8</sub><sup>-</sup> bimetallic cluster

Cite as: J. Vac. Sci. Technol. A **40**, 042201 (2022); doi: 10.1116/6.0001833 Submitted: 25 February 2022 · Accepted: 10 May 2022 ·







#### **AFFILIATIONS**

- Department of Chemistry and Biochemistry, Utah State University, Logan, Utah 84322
- <sup>2</sup>Department of Chemistry, Brown University, Providence, Rhode Island 02912

Note: This manuscript is a part of the Special Topic Collection Commemorating the Career of David Arthur Shirley.

- <sup>a)</sup>Electronic mail: daofu\_yuan@brown.edu
- b) Electronic mail: a.i.boldyrev@usu.edu

Published Online: 27 May 2022

c)Electronic mail: lai-sheng\_wang@brown.edu

#### **ABSTRACT**

Borophenes are atom-thin boron layers that can be grown on coinage metal substrates and have become an important class of synthetic 2D nanomaterials. The interactions between boron and substrates are critical to understand the growth mechanisms of borophenes. Here, we report an investigation of copper-boron interactions in the  $Cu_2B_8^-$  bimetallic cluster using photoelectron spectroscopy and quantum chemical calculations. Well-resolved photoelectron spectra are obtained at several photon energies and are combined with theoretical calculations to elucidate the structures and bonding of  $Cu_2B_8^-$ . Global minimum searches reveal that  $Cu_2B_8^-$  consists of a  $Cu_2$  dimer atop a  $B_8$  molecular wheel with a long Cu-Cu bond length close to that in  $Cu_2^+$ . Chemical bonding analyses indicate that there is clear charge transfer from  $Cu_2$  to  $B_8$ , and the  $Cu_2B_8^-$  cluster can be viewed as a  $[Cu_2^+]$ -borozene complex,  $[Cu_2^+][B_8^{-2}]$ . In the neutral cluster, no Cu-Cu bond exists and  $Cu_2B_8$  consists of two  $Cu^+$  centers interacting with doubly aromatic  $B_8^{-2}$  borozene. The charge transfer interactions between Cu and boron in the  $Cu_2B_8^-$  cluster are analogous to charge transfer from the copper substrate to the first borophene layer recently reported to be critical in the growth of bilayer borophenes on a Cu(111) substrate.

Published under an exclusive license by the AVS. https://doi.org/10.1116/6.0001833

#### I. INTRODUCTION

Boron-based nanotubes were proposed, soon after the discovery of carbon nanotubes, with a triangular boron layer because boron cannot form a honeycomb structure due to its electron deficiency. However, a triangular boron layer is too electron-rich, which induces out-of-plane distortions. Density functional theory (DFT) calculations indicated that a triangular lattice with periodic hexagonal vacancies was more stable and could be perfectly planar, which would be more suitable to construct boron nanotubes. The first experimental evidence of the viability of planar boron sheets came from the systematic investigations of size-selected boron clusters ( $B_n$ ) using photoelectron spectroscopy (PES) and theoretical calculations. Hall small boron clusters were found to possess two-dimensional (2D) structures consisting of  $B_3$  triangles with vacancies of different sizes and are stabilized by

delocalized  $\sigma$  and  $\pi$  bonding within the cluster plane. <sup>11</sup> The B<sub>36</sub> cluster was first found to possess a hexagonal structure with a central hexagonal vacancy, <sup>13</sup> reminiscent of planar boron layers suggested by DFT calculations. <sup>7,8</sup> The name "borophene" was coined for such 2D boron nanostructures, <sup>13</sup> prompted by their experimental viability. The B<sub>35</sub><sup>-</sup> cluster with a double hexagonal vacancy was further found to be an even more flexible motif to construct borophenes. <sup>14</sup> Theoretical calculations suggested that coinage metals would be suitable substrates to grow borophenes <sup>15–17</sup> because boron does not have similar layered bulk polymorphs. Subsequently, borophenes were synthesized on Ag(111) surfaces <sup>18,19</sup> and they are becoming an important class of synthetic 2D nanomaterials. <sup>20,21</sup> The B<sub>48</sub><sup>-</sup> cluster was confirmed to be the first bilayer boron cluster, <sup>22</sup> as suggested theoretically. <sup>23</sup> Recently, bilayer borophenes have also been successfully synthesized on Cu(111) and Ag(111) substrates.

Electron transfers from metal substrates to the first borophene layer were suggested to play an important role in the growth of bilayer borophenes. In addition to coinage metals, borophenes have also been synthesized on Al and Ir substrates, 26,27 albeit the Al substrate gave rise to a honeycomb boron layer due to strong charge transfer. Thus, it is important to study the interactions between boron and the metal substrates at the atomic level, in order to fully understand the growth mechanisms of borophenes.

Extensive research has been done on pure boron and metaldoped boron clusters over the past two decades using joint PES and quantum chemistry calculations <sup>9-14,28,29</sup> as well as ion mobility and infrared spectroscopy. <sup>30,31</sup> The B<sub>7</sub>-, B<sub>8</sub>-, and B<sub>9</sub>- clusters were among the first few boron clusters characterized by PES. 32,33 The  $B_9^-$  cluster was found to have a closed-shell  $D_{8h}$  structure with  $\sigma$ and  $\pi$  double-aromaticity and its unique bonding properties inspired the design of a class of metal-centered borometallic molecular wheels  $(M \odot B_n^{-})$ .  $^{34-36}$  The closed-shell  $B_7^{3-}$  and  $B_8^{2-}$  species, possessing similar double aromaticity, were first realized in AlB<sub>7</sub>, PrB<sub>7</sub>, and LiB<sub>8</sub><sup>-</sup> clusters. The similarity between the  $\pi$  bonding in  $B_7^{3-}$ ,  $B_8^{2-}$ , and  $B_9^{-}$  and that in the prototypical aromatic hydrocarbons, C<sub>5</sub>H<sub>5</sub><sup>-</sup>, C<sub>6</sub>H<sub>6</sub>, and C<sub>7</sub>H<sub>7</sub><sup>+</sup>, was recognized in a recent study on lanthanide octa-boron clusters (LnB<sub>8</sub><sup>-</sup>), and a name "borozene" was proposed for the wheel-like aromatic boron clusters. Among the three borozenes, B<sub>8</sub><sup>2-</sup> is unique for its high stability and has been observed in several metal-doped boron clusters (MB<sub>8</sub><sup>-1/0</sup>).<sup>37</sup> Even though transition-metal-doped MB<sub>8</sub><sup>-</sup> clusters are dominated by metal-centered molecular wheels (M©B<sub>8</sub><sup>-</sup>), 34-36,42-44 the MB<sub>8</sub> species with metals of low electronegativities have been shown to form charge-transfer complexes as a result of the high stability of the B<sub>8</sub><sup>2</sup> borozene. 37,39,45 The recent results on BiB<sub>8</sub> and AuB<sub>8</sub> provide new examples of metal-borozene complexes. 45

Despite recent advances on mono-metal-doped boron clusters, <sup>28,36,47</sup> di-metal-doped boron clusters remain relatively unexplored experimentally. <sup>12,29</sup> Di-gold-doped boron clusters  $B_x A u_2^{0/-}$  (x = 3, 6, and 7) were found to follow the double-chain motifs with terminal Au atoms. 48-50 Di-tantalum-doped boron clusters  $Ta_2B_x^-$  (x = 2-6) were shown to consist of a  $Ta_2$  dimer with boron atoms building around it.51,52 Di-lanthanide boron clusters  $\text{Ln}_2\text{B}_x^-$  (x = 7–9) were found to possess inverse-sandwich structures with a monocyclic B<sub>x</sub> ring, instead of Ln<sub>2</sub>-borozene complexes.<sup>53,54</sup> Several transition metal M<sub>2</sub>B<sub>8</sub> species were also suggested to have inverse-sandwich-type structures,<sup>29</sup> whereas M<sub>2</sub>B<sub>8</sub> (M = Mg, Zn, Cd, and Hg) species were predicted to be M<sub>2</sub>-borozene complexes. 55-57 In the current article, we present a joint PES and quantum chemical study on the Cu<sub>2</sub>B<sub>8</sub><sup>-</sup> cluster to probe the copper-boron interactions. Specifically, we are interested in whether there would be strong charge transfer from copper to boron and whether it would form a borozene complex or an inverse-sandwich-type structure. The photoelectron spectra taken at different photon energies are well-resolved and are used to elucidate the structures and bonding in Cu<sub>2</sub>B<sub>8</sub><sup>-</sup> and its neutral. Strong charge transfers are observed from Cu2 to B8 and the global minimum of Cu<sub>2</sub>B<sub>8</sub><sup>-</sup> is found to feature a Cu<sub>2</sub><sup>+</sup> dimer atop the B<sub>8</sub><sup>2-</sup> borozene surface. The neutral Cu<sub>2</sub>B<sub>8</sub> cluster is shown to consist of two Cu<sup>+</sup> centers interacting with B<sub>8</sub><sup>2-</sup> borozene without Cu-Cu bonding. The charge transfer interactions between copper and boron in the bimetallic clusters are similar to those from the

copper substrate to the first borophene layer suggested to be critical for the growth of bilayer borophenes on a Cu(111) surface.

#### II. EXPERIMENTAL AND THEORETICAL METHODS

#### A. Photoelectron spectroscopy

The experiment was performed with a PES apparatus consisting of a laser vaporization supersonic cluster source, a time-of-flight (TOF) mass spectrometer, and a magnetic-bottle photoelectron analyzer, details of which can be found elsewhere.<sup>1</sup> The Cu<sub>2</sub>B<sub>8</sub><sup>-</sup> cluster was produced by laser ablation of a mixed Cu-B disk target, prepared from a Cu powder (natural isotopes) and a <sup>11</sup>B-enriched (97%) boron powder. The laser-induced plasma was quenched by a pulsed helium carrier gas seeded with 5% argon, initiating nucleation. Clusters formed inside the nozzle were entrained by the carrier gas and underwent supersonic expansion. After passing through a skimmer, negatively charged clusters in the collimated beam were accelerated perpendicularly into the TOF mass spectrometer. The Cu<sub>2</sub>B<sub>8</sub><sup>-</sup> cluster was mass-selected and decelerated before crossing with the detachment laser beam. Three different detachment laser wavelengths were used, including the 193.0 nm (6.424 eV) radiation from an ArF excimer laser and the third harmonics (354.7 nm, 3.496 eV) and fourth harmonics (266.0 nm, 4.661 eV) of a Nd:YAG laser. Photoelectrons were collected with over 90% efficiency by the magnetic bottle and analyzed in a 3.5 m long electron TOF tube. The photoelectron kinetic energies were calibrated using the known transitions of the Bi atomic anion. The kinetic energy  $(E_k)$  resolution  $(\Delta E_k/E_k)$  of the magneticbottle photoelectron analyzer was about 2.5%, that is, ~25 meV for electrons with 1 eV kinetic energy.

#### **B.** Theoretical methods

We performed extensive global minimum (GM) searches for the Cu<sub>2</sub>B<sub>8</sub> anion and the neutral Cu<sub>2</sub>B<sub>8</sub> cluster using the AFFCK global optimization method,<sup>58</sup> which involved an intermediate optimization step with a classical force field. More than 3300 starting geometries were generated for Cu<sub>2</sub>B<sub>8</sub><sup>-</sup> during the GM search. After the initial optimization at the PBE0/def2svp level, 59,60 the low-lying isomers were reoptimized and ordered at the PBE0/aug-cc-pVTZ + ZPE and CCSD(T)/aug-cc-pVTZ//PBE0/ aug-cc-pVTZ levels of theory as implemented in Gaussian-16.61 Both doublet and quartet states for Cu<sub>2</sub>B<sub>8</sub><sup>-</sup> were tested for each generated structure. Similar GM searches were done for Cu<sub>2</sub>B<sub>8</sub> neutral clusters. Vertical detachment energies (VDEs) and the adiabatic detachment energy (ADE) for the GM of Cu<sub>2</sub>B<sub>8</sub> were calculated using two approaches: (1) time-dependent DFT (TD-DFT) at the PBE0/aug-cc-pVTZ level of theory and (2) the more accurate CCSD(T)/aug-cc-pVTZ method. The first VDE was calculated as the energy difference between the neutral and anion at optimized anion geometry. The ADE was computed as the energy difference between the optimized anion and the optimized neutral starting from the corresponding anion structure. The inclusion of scalar relativistic corrections at the PBE0/ZORA-def2-TZVP level, as implemented in the ORCA package, <sup>64</sup> did not change the relative order of isomers and had negligible effects on calculated VDEs.

Chemical bonding of  $\mathrm{Cu_2B_8}^-$  and  $\mathrm{Cu_2B_8}$  clusters was analyzed using molecular orbital (MO) analyses as well as the Adaptive Natural Density Partitioning (AdNDP) method<sup>65</sup> as an effective probe for deciphering bonding in complicated doped clusters <sup>66,67</sup> and other complex systems with electron delocalization. <sup>68–70</sup> The AdNDP algorithm was a generalization of the natural bonding orbital (NBO) analysis and was based on the diagonalization of the blocks of the first-order density matrix in the basis of natural atomic orbitals. The AdNDP approach works within the concept of occupation numbers, such that a reliable bonding picture should exhibit bond occupancies close to 2.0 (1.0 for one-electron bonds) and agree with overall electron counting.

#### III. RESULTS

#### A. Experimental results

The photoelectron spectra of Cu<sub>2</sub>B<sub>8</sub><sup>-</sup> at different wavelengths are shown in Fig. 1. The spectra are well resolved with distinct features labeled as X, and A to F. Band X refers to detachment transition from the ground state of Cu<sub>2</sub>B<sub>8</sub><sup>-</sup> to that of neutral Cu<sub>2</sub>B<sub>8</sub>, while the bands at higher binding energies represent transitions to excited states of neutral Cu<sub>2</sub>B<sub>8</sub>. The first VDE of Cu<sub>2</sub>B<sub>8</sub><sup>-</sup> is obtained from band X as 2.80 eV and the ADE is estimated from the onset of band X to be 2.65 eV, which also represents the electron affinity of neutral Cu<sub>2</sub>B<sub>8</sub>. A sharp and intense band A is observed at 3.34 eV in the 266 nm spectrum, which is partially cut off in the 355 nm spectrum, followed by a weaker band B at 3.53 eV. The 266 nm spectrum also reveals a broader band C at a VDE of 3.88 eV. Two strong bands D (VDE: 4.64 eV) and E (VDE: 4.91 eV) are resolved in the 193 nm spectrum, following an energy gap. Highly congested spectral features are observed beyond 5 eV and are labeled as F for the sake of discussion. Due to the isotopic distribution of copper, the mass spectrum is rather congested and contaminations are observed, as indicated by weak features labeled by asterisks at low binding energies in Fig. 1. The most likely contaminant around the mass of Cu<sub>2</sub>B<sub>8</sub> was Cu<sub>3</sub>B<sub>2</sub> because of the isotopic distributions of Cu even though <sup>11</sup>B-enriched boron was used. The binding energies of all the observed spectral features are given in Table S1<sup>74</sup> in comparison to the TD-DFT results.

#### **B.** Theoretical results

#### 1. Global minimum search for the Cu<sub>2</sub>B<sub>8</sub> anion

The structures found within 20 kcal/mol of the global minimum are shown in Fig. 2. According to both PBE0 and CCSD (T), the GM of  $\text{Cu}_2\text{B}_8^-$  is a  $C_s$  ( $^2\text{A}'$ ) structure composed of a  $\text{B}_8$  wheel and a  $\text{Cu}_2$  dimer atop the boron plane. The B–B distances in the  $\text{B}_8$  motif are 1.55–1.54 Å for the periphery and 1.79 Å for radial bonds, almost identical to those in bare  $D_{7h}$  doubly aromatic  $\text{B}_8^{2-}$  borozene. These structural parameters suggest that there must be significant charge transfer from  $\text{Cu}_2$  to the  $\text{B}_8$  moiety to fulfill its double aromaticity. The computed Cu–Cu distance in  $\text{Cu}_2\text{B}_8^-$  is 2.42 Å, much longer than the calculated Cu–Cu distance of 2.22 Å for isolated  $\text{Cu}_2$ . However, the Cu–Cu distance in  $\text{Cu}_2\text{B}_8^-$  is similar to that of 2.46 Å in  $\text{Cu}_2^+$ , suggesting that one electron is transferred from the  $\text{Cu}_2$  dimer to  $\text{B}_8$  in  $\text{Cu}_2\text{B}_8^-$ , which can be viewed as a  $[\text{Cu}_2^+]$ -borozene complex,  $[\text{Cu}_2^+]$ [ $\text{B}_8^{2-}$ ]. The distances between

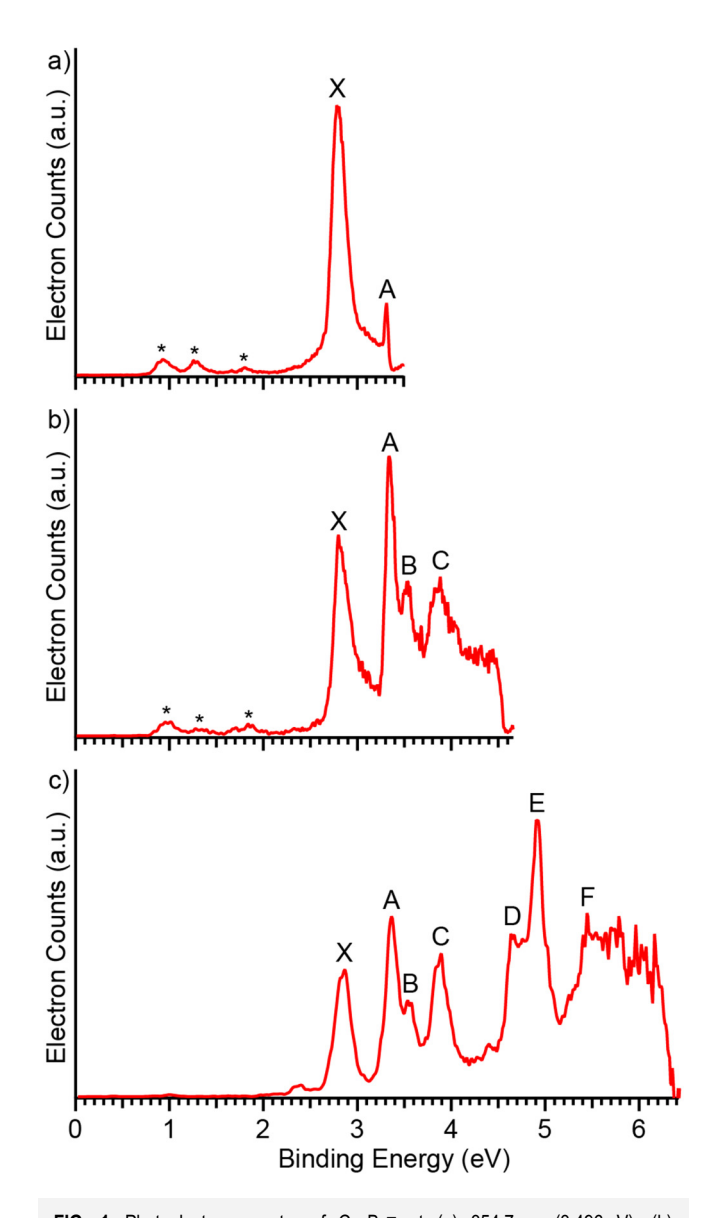


**FIG. 1.** Photoelectron spectra of  $\rm Cu_2B_8^-$  at (a) 354.7 nm (3.496 eV), (b) 266.0 nm (4.661 eV), and (c) 193.0 nm (6.424 eV). The weak features labeled with \* are due to contaminations.

the Cu atoms and the B atoms are between 2.13–2.19 Å, longer than a single Cu–B bond distance based on the atomic covalent radii of Pyykkö (1.97 Å). This observation again is consistent with relatively weak interactions between Cu<sub>2</sub> and the B<sub>8</sub> moiety.

The nearest low-lying isomer of  $\text{Cu}_2\text{B}_8^-$  (Iso1) has an inverse sandwich structure, which is  $10.6\,\text{kcal/mol}$  higher in energy at the PBE0 level and  $5.1\,\text{kcal/mol}$  higher at the CCSD(T) level above the GM. Iso2 and Iso3 both involve a quasi-planar  $\text{B}_8$  interacting with two separated Cu atoms, whereas Iso4 features a three-dimensional (3D)  $\text{B}_8$  motif interacting with a Cu<sub>2</sub> dimer.

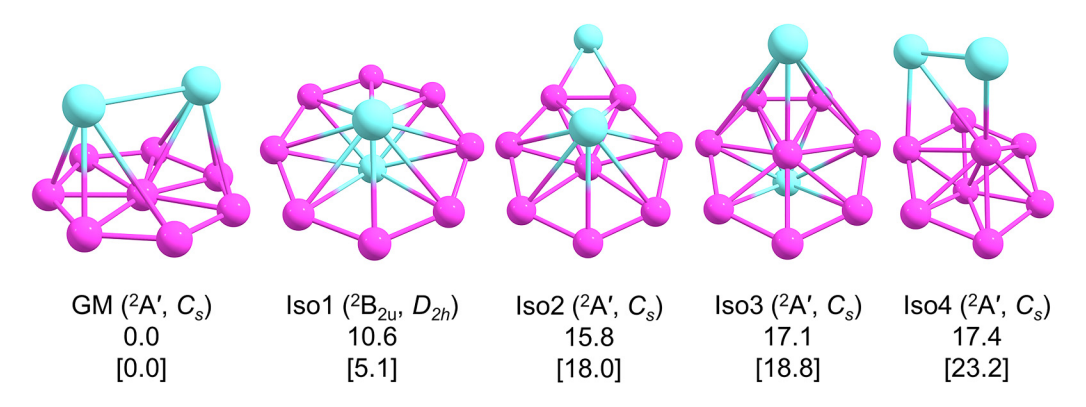


FIG. 2. Global minimum and low-lying isomers of  $Cu_2B_8^-$  and their relative energies in kcal/mol at PBE0/aug-cc-pVTZ and CCSD(T)/aug-cc-pVTZ//PBE0/aug-cc-pVTZ (in brackets) levels. The Cartesian coordinates of these structures are given in Table S2 (Ref. 74).

## 2. Global minimum search for the $Cu_2B_8$ neutral cluster

Removing the extra electron from the GM of  $Cu_2B_8^-$  leads to a large increase in the Cu–Cu distance (2.58 Å) in the neutral  $Cu_2B_8$  final state (FS in Fig. 3), suggesting that there is no formal Cu–Cu bond. Global minimum searches reveal that the GM of  $Cu_2B_8$ , in fact, involves a  $B_8$  wheel with two separated Cu atoms, one above the boron plane and another bonded to the edge (GM in Fig. 3). Iso1, which is also more stable than FS, features two separated Cu atoms, one above and one below the  $B_8$  plane. Iso2 and Iso3, which are higher in energy than the FS, both feature 3D  $B_8$  motifs. The three lowest-lying isomers of neutral  $Cu_2B_8$  (FS, GM, and Iso1) are close in energy and all consist of the  $B_8$  wheel interacting with two separated Cu atoms, suggesting the high stability of the borozene motif.

#### IV. DISCUSSION

#### A. Comparison between experiment and theory

We have analyzed the MOs (Fig. S1) $^{74}$  and computed the VDEs for the GM of  $\text{Cu}_2\text{B}_8^-$  to help interpret the photoelectron

spectra. The first detachment channel (X) is from the 21a' singly occupied MO (SOMO), which is a Cu-Cu bonding orbital primarily composed of Cu 4s atomic orbitals (AOs). The calculated VDE of 2.75 eV at the CCSD(T) level is in excellent agreement with the experimental value of 2.80 eV, as shown in Table I. The computed ADE of 2.45 eV is also consistent with the experimental estimate of 2.65 eV. The removal of the Cu-Cu bonding electron in the anion leads to a large increase in the Cu-Cu distance in the final state (FS in Fig. 3), consistent with the relatively broad PES peak X and the large difference between the ADE and VDE. The ground state band X was not better resolved even in the 355 nm spectrum [Fig. 1(a)] because it should contain broad low-frequency Cu-Cu stretching vibrational progression with a computed frequency of 119.29 cm<sup>-1</sup> significantly reduced relative to that in the  $\text{Cu}_2\text{B}_8^-$  anion (179.40 cm $^{-1}$ ). Electron detachment from the HOMO (11a") (Fig. S1)<sup>74</sup> results in two detachment channels, <sup>3</sup>A" and <sup>1</sup>A", with computed VDEs of 3.37 and 3.46 eV at the CCSD(T) level, in excellent agreement with the measured VDEs for A and B bands, respectively, as seen in Table I. The relative intensities of A and B bands agree well with the spin multiplicities of the <sup>3</sup>A" and <sup>1</sup>A"

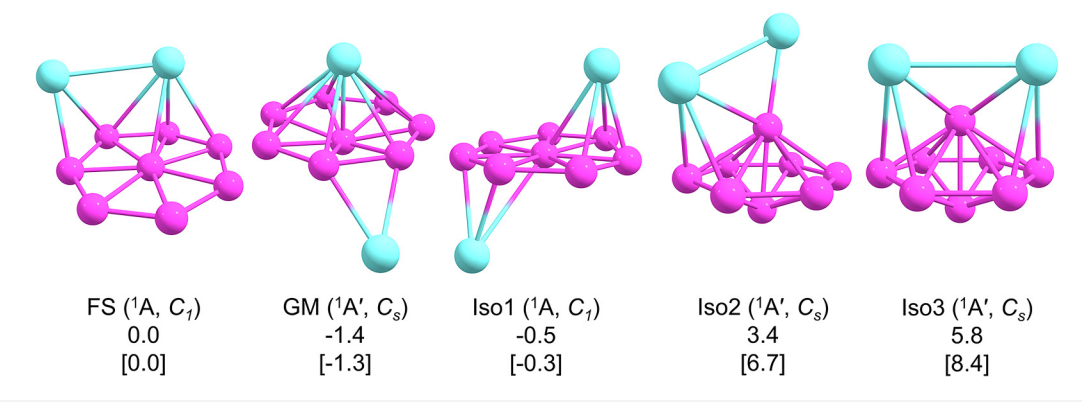


FIG. 3. Global minimum and low-lying isomers of  $Cu_2B_8$  and their relative energies in kcal/mol at PBE0/aug-cc-pVTZ and CCSD(T)/aug-cc-pVTZ/PBE0/aug-cc-pVTZ (in brackets) levels. Note the GM of neutral  $Cu_2B_8$  is different from that of the anion (Fig. 2). The Cartesian coordinates of these structures are given in Table S3 (Ref. 74).

**TABLE I.** Comparison of the experimental ADE and VDEs of  $Cu_2B_8^-$  with calculated values at the CCSD(T)/aug-cc-pVTZ level of theory for the GM  $C_s$  ( $^2$ A') structure. All energies are in eV.

	VDE/ADE (exp.) <sup>a</sup>	Final state and electron configuration	VDE/ADE (theo)
X A B	2.80/2.65 3.34 3.53 3.88	$^{1}A' \{(20a')^{2}(11a'')^{2}(21a')^{0}\}$ $^{3}A'' \{(20a')^{2}(11a'')^{1}(21a')^{1}\}$ $^{1}A'' \{(20a')^{2}(11a'')^{1}(21a')^{1}\}$ $^{3}A' \{(20a')^{1}(11a'')^{2}(21a')^{1}\}$	2.75/2.45 3.37 3.46 3.91

<sup>&</sup>lt;sup>a</sup>The experimental uncertainty was estimated to be ±0.03 eV.

final states. Electron detachment from the HOMO-1 (20a') gives rise to two final states, <sup>3</sup>A' and <sup>1</sup>A'. The computed VDE for the <sup>3</sup>A' state of 3.91 eV at the CCSD(T) level agrees well with band C at 3.88 eV. Unfortunately, the CCSD(T) method cannot be used to compute the VDE of the <sup>1</sup>A' excited state because it has the same symmetry as the ground state. The calculations of higher VDEs within the CCSD(T) formalism can be done by swapping LUMO and HOMO-n in a neutral system, which result in SCF convergence to excited electronic states. However, swapping of LUMO and HOMO-n that are of the same symmetry does not change the overall wavefunction symmetry and results in convergence to the same lowest energy state corresponding to this specific wavefunction symmetry. For same symmetry reasons, the CCST(T) method cannot be used to compute the VDEs of any higher detachment channels. The CCSD(T) VDEs are also compared with the 266 nm spectrum in Fig. 4.

Therefore, we used the TD-DFT approach to compute all the VDEs up to the binding energies probed at 193 nm, as given in

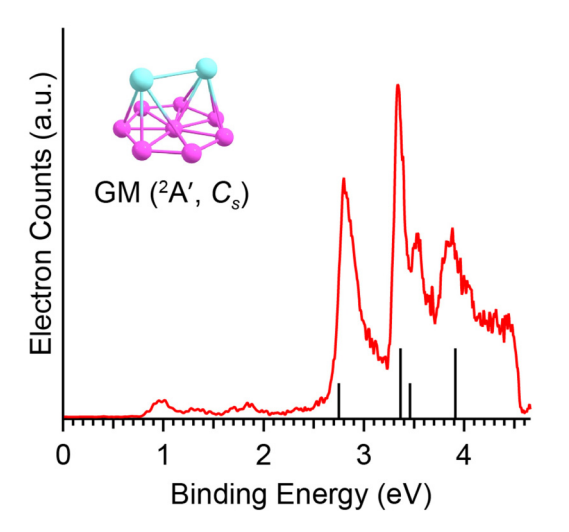


**FIG. 4.** Comparison of the computed VDEs with the photoelectron spectrum of  $\text{Cu}_2\text{B}_8^-$  at 266 nm. The vertical bars correspond to computed VDEs at the CCSD(T)/aug-cc-pVTZ level of theory. The longer and shorter bars correspond to transitions to triplet and singlet final states, respectively (see Table I).

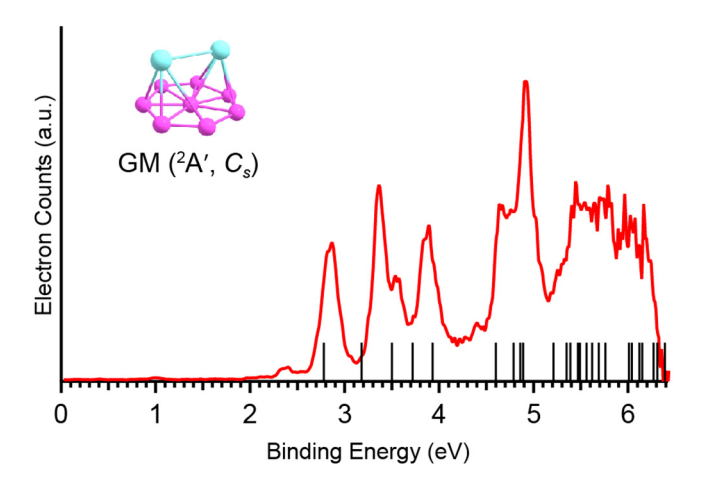


**FIG. 5.** Comparison of the computed VDEs with the photoelectron spectrum of  $\text{Cu}_2\text{B}_8^-$  at 193 nm. The vertical bars correspond to computed VDEs at the TD-DFT level of theory [see Table S1 (Ref. 74)].

Table S1<sup>74</sup> and shown in Fig. 5. DFT is not a truly ab initio method since its exchange-correlation part is usually empirically fitted. Among a plethora of DFT exchange-correlation functionals, we used PBE0, which is a time-proven DFT functional for doped boron clusters. The PBE0 functional does not contain empirical parameters and its exchange-correlation part is fitted using fundamental constants only. Even though the TD-DFT results are less accurate than those from CCSD(T), they give qualitative understanding of high binding energy PES features. As seen from MOs in Fig. S1,<sup>74</sup> the HOMO, HOMO-1 to HOMO-3 involve  $\pi$  or  $\sigma$ bonding in the B<sub>8</sub> motif with minor contributions from Cu 3d AOs, corresponding to the discrete PES features observed between 3 and 5 eV. The HOMO-4 to HOMO-13 are basically nonbonding Cu 3d AOs, which should give rise to congested spectral features, in agreement with the almost continuous PES signals beyond 5 eV. The excellent agreement between the CCSD(T) results and the experimental data and the good agreement between the TD-DFT results and the overall spectral pattern provide unequivocal confirmation for the GM of Cu<sub>2</sub>B<sub>8</sub><sup>-</sup>.

## B. Chemical bonding in $Cu_2B_8^-$ : $Cu_2^+$ on the $B_8^{2-}$ borozene surface

Compared to MO analyses displayed in Fig. S1, <sup>74</sup> the overall bonding picture in  $\text{Cu}_2\text{B}_8^-$  is recovered better via the AdNDP analysis, as shown in Fig. 6. Because of the nonbonding nature of the Cu 3d<sup>10</sup> AOs (Fig. S1), <sup>74</sup> each Cu atom in  $\text{Cu}_2\text{B}_8^-$  contains five 3d lone pairs represented as 1c-2e bonds, which are omitted from Fig. 6 (see Fig. S2). <sup>74</sup> The AdNDP analysis revealed a 2c-1e Cu–Cu  $\sigma$  bond (bond order = ½) and seven 2c-2e B–B  $\sigma$  bonds on the periphery of the B<sub>8</sub> motif [Fig. 6(a)], three 8c-2e delocalized  $\sigma$  bonds on the B<sub>8</sub> wheel [Fig. 6(b)], and three 10c-2e delocalized  $\sigma$  bonds [Fig. 6(c)], which are mainly centered on the B<sub>8</sub> wheel. It is known that the neutral B<sub>8</sub> cluster has a triplet ground state with two unpaired electrons occupying two degenerate  $\pi$  MOs. <sup>33</sup> Adding

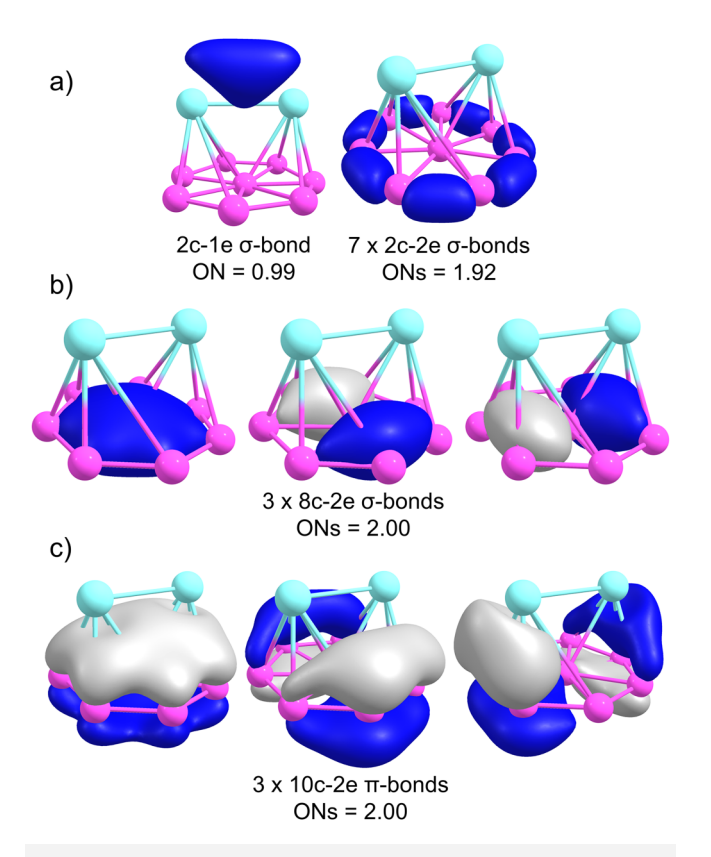


**FIG. 6.** AdNDP bonding analysis for Cu<sub>2</sub>B<sub>8</sub><sup>-.</sup> (a) The 2c-1e Cu–Cu  $\sigma$ -bond and seven 2c-2e B–B  $\sigma$ -bonds. (b) Three 8c-2e delocalized  $\sigma$ -bonds. (c) Three 10c-2e  $\pi$ -aromatic bonds. ON stands for occupation number. Note the ten Cu 3d 1c-2e lone pairs are omitted.

two electrons to  $B_8$  results in the closed-shell  ${B_8}^{2^-}$  species with six delocalized  $\sigma$  electrons and six delocalized  $\pi$  electrons, both satisfying the 4N+2 Hückel rule for aromaticity. The doubly ( $\sigma$  and  $\pi$ ) aromatic  ${B_8}^{2^-}$  is known as borozene.  $^{40}$  The double  $\sigma$  and  $\pi$  aromaticity in the  ${B_8}^{2^-}$  motif, manifested by three delocalized  $\sigma$  and  $\pi$  bonds, is maintained in  $\text{Cu}_2{B_8}^-$ . A charge is transferred from  $\text{Cu}_2$  to the  $B_8$  motif to fulfill the double aromaticity of  ${B_8}^{2^-}$  borozene, while reducing the bond order on the  $\text{Cu}_2$  dimer.

It is important to note that there is no direct Cu–B covalent bonding, indicating that the two Cu atoms interact with the  $B_8$  motif primarily via ionic bonding, and thus, the  $\text{Cu}_2\text{B}_8^-$  cluster can be viewed as a  $[\text{Cu}_2^+][B_8^{\ 2^-}]$  borozene complex. Although we include the two Cu atoms in the AdNDP results for the delocalized  $\pi$  bonds, their contributions to the occupation numbers are quite small, ~10%. The weak  $\text{Cu}_2\text{-B}_8$   $\pi$  bonding can be glimpsed in the HOMO-1 (20a') (Fig. S1). The bonding in the  $\text{Cu}_2\text{B}_8^-$  cluster is reminiscent of the lanthanide-borozene complexes,  $[\text{Ln}^+][B_8^{\ 2^-}]$  as well as that in the  $[M_2]^{2^+}[B_8^{\ 2^-}]$  clusters (M = Mg or group IIB elements), which were investigated computationally. The sum of these metals is their low electronegativity, which

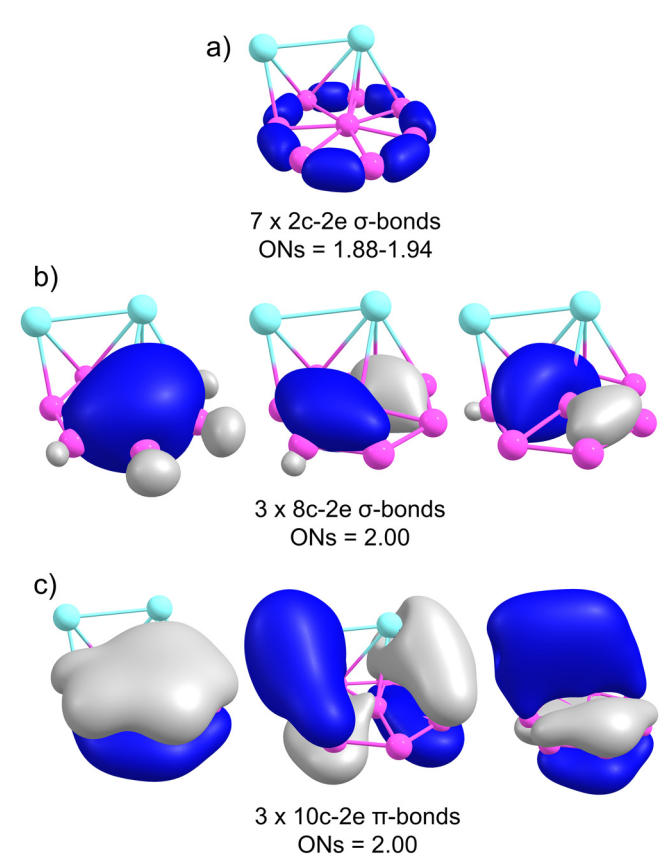


**FIG. 7.** AdNDP bonding analysis for the final state of Cu<sub>2</sub>B<sub>8</sub> upon electron detachment from the GM of the anion. (a) Seven 2c-2e B–B  $\sigma$ -bonds. (b) Three 8c-2e  $\sigma$ -aromatic bonds. (c) Three 10c-2e  $\pi$ -aromatic bonds. ON stands for occupation number. Note that the ten Cu 3d 1c-2e lone pairs are omitted.

facilitates charge transfer to  $B_8$  and is critical to maintain the doubly aromatic  $B_8^{\,2-}$  borozene. Strong covalent interactions between the heteroatom and boron would distort the  $B_8$  wheel structure, such as in  $H_2B_8^{\,-}$  or  $B_8(BO)_2^{\,-,72,73}$  where the  $B_8$  motif is elongated to a double chain structure to favor the formation of two terminal B–H or B–BO bonds, respectively.

The NBO analysis reveals that that the  $Cu_2$  unit carries a positive charge of +0.5 |e| while that on the  $B_8$  fragment is -1.5 |e|, consistent with  $[Cu_2]^+[B_8^{\;2-}]$  formulation. From a quantitative point of view, this indicates that a copper dimer donates 0.5 |e| to the boron wheel within the NBO scheme. In a discrete formalism, as provided by AdNDP, one of the two s-electrons is withdrawn from the  $Cu_2$  dimer to fulfill the aromatic condition of the  $B_8^{\;2-}$  borozene.

According to the recent synthesis of bilayer borophenes on a copper substrate,  $^{24}$  there is significant charge transfer from the copper substrate to the first layer of borophene, which is critical for the ordered nucleation of the second boron layer and key for the formation of bilayer borophenes. Similar charge transfer from Cu to boron is also manifested in the  $\text{Cu}_2\text{B}_8^-$  bimetallic cluster.



## C. Chemical bonding in $\text{Cu}_2\text{B}_8$ :Cu atoms on the borozene surface

The removal of the Cu-Cu bonding electron in the SOMO of Cu<sub>2</sub>B<sub>8</sub> leads to a large increase in the Cu-Cu bond length in the final state of  $Cu_2B_8$  (FS in Fig. 3) and destroys the ½ Cu-Cu  $\sigma$ bond, as shown in the AdNDP analysis in Fig. 7. The Cu<sub>2</sub>B<sub>8</sub> cluster can be viewed as two Cu<sup>+</sup> centers interacting ionically with the doubly aromatic  $B_8^{2-}$  borozene, i.e.,  $[Cu^+]_2[B_8^{2-}]$ . The large Coulomb repulsion due to the proximity of the two Cu<sup>+</sup> centers in the final state of Cu<sub>2</sub>B<sub>8</sub> explains why it is not the global minimum on the potential energy surface of the neutral system. Both the GM and Iso1 of Cu2B8, which are slightly lower in energy, consist of two separated copper atoms interacting with the B<sub>8</sub> motif, as shown in Fig. 3. The AdNDP bonding analysis confirms that the GM of Cu<sub>2</sub>B<sub>8</sub> is also composed of two Cu<sup>+</sup> centers interacting with a doubly aromatic B<sub>8</sub><sup>2-</sup> borozene, as shown in Fig. S3.<sup>74</sup> It should be noted that the first three structures of neutral Cu<sub>2</sub>B<sub>8</sub> (FS, GM, and Iso1 in Fig. 3) are all close in energy [within 1.3 kcal/mol of each other at the CCSD(T) level], consistent with ionic interactions between the two Cu+ centers and the borozene surface. In the GM of Cu<sub>2</sub>B<sub>8</sub>, the  $\eta^8$ -Cu<sup>+</sup> center enjoys optimal interactions with the borozene, whereas in Iso1 the two Cu+ centers are positioned as far as possible.

#### V. CONCLUSIONS

We report an investigation on the structures and bonding of the Cu<sub>2</sub>B<sub>8</sub> bimetallic cluster using photoelectron spectroscopy and quantum chemical calculations. The global minimum of Cu<sub>2</sub>B<sub>8</sub><sup>-</sup> was found to be a B<sub>8</sub> wheel with a Cu<sub>2</sub> dimer atop the boron plane. The copper dimer donates one electron to the B<sub>8</sub> motif to fulfill double aromaticity of the B<sub>8</sub><sup>2-</sup> borozene, whereas the Cu<sub>2</sub> dimer becomes Cu<sub>2</sub><sup>+</sup> with a one-electron Cu-Cu bond. The copper dimer is not involved in direct covalent bonding with boron and is weakly bonded to the B<sub>8</sub> motif via ionic interactions, forming a Cu<sub>2</sub><sup>+</sup> borozene complex,  $[Cu_2^+][B_8^{\ 2^-}]$ . The removal of the extra electron in the anion results in a neutral Cu<sub>2</sub>B<sub>8</sub> cluster, which contains no Cu-Cu bonding. Instead, the global minimum and low-lying isomers of Cu<sub>2</sub>B<sub>8</sub> consist of two Cu<sup>+</sup> centers interacting with the doubly aromatic B<sub>8</sub><sup>2-</sup> borozene. The current results not only confirm again the high stability of the doubly aromatic B<sub>8</sub><sup>2-</sup> borozene, but also provide insight into how copper interacts with boron surfaces, which is critical to understand copper as an important substrate for the growth of borophenes.

#### **ACKNOWLEDGMENTS**

This work was supported by the National Science Foundation (NSF) (No. CHE-2053541 to L.S.W.). Computational resources were provided by the Center for High Performance Computing at the University of Utah. This work was done specifically in the memory of Professor David A. Shirley. One of us (L.S.W.) still fondly recalls his first meeting with Dave as a first-year graduate student when Dave described his Ph.D. project to him: to study  $Cu_2$  ( $Cu + Cu \rightarrow Cu_2$ ) and larger copper clusters using a high-temperature molecular beam source and HeI photoelectron spectroscopy. While the  $Cu_2$  project proved to be ahead of its time, he

hopes that Dave would be pleased that it is now possible to study  $\text{Cu}_2$  on the microscopic surface of a planar boron cluster using photoelectron spectroscopy.

#### **AUTHOR DECLARATIONS**

#### **Conflict of Interest**

The authors have no conflicts to disclose.

#### **Author Contributions**

M.K. and W.-J.C. contributed equally to this work.

#### **DATA AVAILABILITY**

The data that support the findings of this study are available within the article and its supplementary material.<sup>74</sup>

#### **REFERENCES**

- <sup>1</sup>A. Gindulyte, W. N. Lipscomb, and N. L. Massa, Inorg. Chem. 37, 6544 (1998).
- <sup>2</sup>I. Boustani and A. Quandt, Europhys. Lett. **39**, 527 (1997).
- <sup>3</sup>I. Boustani, A. Quandt, E. Hernandez, and A. Rubio, J. Chem. Phys. 110, 3176 (1999).
- <sup>4</sup>M. H. Evans, J. D. Joannopoulos, and S. T. Pantelides, Phys. Rev. B 72, 045434 (2005).
- <sup>5</sup>J. Kunstmann and A. Quandt, Phys. Rev. B 74, 035413 (2006).
- <sup>6</sup>K. C. Lau and R. Pandey, J. Phys. Chem. C 111, 2906 (2007).
- <sup>7</sup>H. Tang and S. Ismail-Beigi, Phys. Rev. Lett. **99**, 115501 (2007).
- <sup>8</sup>X. Yang, Y. Ding, and J. Ni, Phys. Rev. B 77, 041402 (2008).
- <sup>9</sup>A. N. Alexandrova, A. I. Boldyrev, H. J. Zhai, and L. S. Wang, Coord. Chem. Rev. 250, 2811 (2006).
- <sup>10</sup>A. P. Sergeeva, I. A. Popov, Z. A. Piazza, W. L. Li, C. Romanescu, L. S. Wang, and A. I. Boldyrev, Acc. Chem. Res. 47, 1349 (2014).
- <sup>11</sup>L. S. Wang, Int. Rev. Phys. Chem. **35**, 69 (2016).
- 12 T. Jian, X. Chen, S. D. Li, A. I. Boldyrev, J. Li, and L. S. Wang, Chem. Soc. Rev. 48, 3550 (2019).
- <sup>13</sup>Z. A. Piazza, H. S. Hu, W. L. Li, Y. F. Zhao, J. Li, and L. S. Wang, Nat. Commun. 5, 3113 (2014).
- 14W.-L. Li et al., J. Am. Chem. Soc. 136, 12257 (2014).
- 15Y. Liu, E. S. Penev, and B. I. Yakobson, Angew. Chem. Int. Ed. 52, 3156 (2013).
- <sup>16</sup>H. Liu, J. Gao, and J. Zhao, Sci. Rep. 3, 3228 (2013).
- 17Z. Zhang, Y. Yang, G. Gao, and B. I. Yakobson, Angew. Chem. Int. Ed. 54, 13022 (2015).
- <sup>18</sup>A. J. Mannix et al., Science **350**, 1513 (2015).
- 19B. Feng et al., Nat. Chem. 8, 563 (2016).
- <sup>20</sup>S. Y. Xie, Y. L. Wang, and X. B. Li, Adv. Mater. 31, 1900392 (2019).
- <sup>21</sup>S. Yadav, M. A. Sadique, A. Kaushik, P. Ranjan, R. Khan, and A. K. Srivastava, J. Mater. Chem. B 10, 1146 (2022).
- <sup>22</sup>W. J. Chen et al., Nanoscale 13, 3868 (2021).
- <sup>23</sup>L. Sai, X. Wu, N. Gao, J. Zhao, and R. B. King, Nanoscale 9, 13905 (2017).
- 24 C. Chen et al., Nat. Chem. 14, 25 (2022).
- 25X. Liu, Q. Li, Q. Ruan, M. S. Rahn, B. I. Yakobson, and M. C. Hersam, Nat. Mater. 21, 35 (2022).
- 26W. Li et al., Sci. Bull. 63, 282 (2018).
- 27N. A. Vinogradov, A. Lyalin, T. Taketsugu, A. S. Vinogradov, and A. Preobrajenski, ACS Nano 13, 14511 (2019).
- <sup>28</sup>W. L. Li, X. Chen, T. Jian, T. T. Chen, J. Li, and L. S. Wang, Nat. Rev. Chem. 1, 0071 (2017).
- <sup>29</sup>J. Barroso, S. Pan, and G. Merino, Chem. Soc. Rev. 51, 1098 (2022).



- <sup>30</sup>E. Oger, N. R. M. Crawford, R. Kelting, P. Weis, M. M. Kappes, and R. Ahlrichs, Angew. Chem. Int. Ed. 46, 8503 (2007).
- <sup>31</sup>S. Pan, J. Barroso, S. Jalife, T. Heine, K. R. Asmis, and G. Merino, Acc. Chem. Res. 52, 2732 (2019).
- <sup>32</sup>A. N. Alexandrova, A. I. Boldyrev, H. J. Zhai, and L. S. Wang, J. Phys. Chem. A 108, 3509 (2004).
- <sup>33</sup>H. J. Zhai, A. N. Alexandrova, K. A. Birch, A. I. Boldyrev, and L. S. Wang, Angew. Chem. Int. Ed. 42, 6004 (2003).
- <sup>34</sup>C. Romanescu, T. R. Galeev, W. L. Li, A. I. Boldyrev, and L. S. Wang, Angew. Chem. 123, 9506 (2011).
- 35T. R. Galeev, C. Romanescu, W. L. Li, L. S. Wang, and A. I. Boldyrev, Angew. Chem. Int. Ed. 51, 2101 (2012).
- <sup>36</sup>C. Romanescu, T. R. Galeev, W. L. Li, A. I. Boldyrev, and L. S. Wang, Acc. Chem. Res. 46, 350 (2013).
- Chem. Res. 46, 350 (2013).
   T. R. Galeev, C. Romanescu, W. L. Li, L. S. Wang, and A. I. Boldyrev, J. Chem.
   Phys. 135, 104301 (2011).
- <sup>38</sup>T. T. Chen, W. L. Li, T. Jian, X. Chen, J. Li, and L. S. Wang, Angew. Chem. Int. Ed. 56, 6916 (2017).
- <sup>39</sup> A. N. Alexandrova, H. J. Zhai, L. S. Wang, and A. I. Boldyrev, Inorg. Chem. 43, 3552 (2004).
- <sup>40</sup>W. L. Li, T. T. Chen, W. J. Chen, J. Li, and L. S. Wang, Nat. Commun. 12, 6467 (2021).
- <sup>41</sup>L. M. Wang, W. Huang, B. B. Averkiev, A. I. Boldyrev, A. I. Boldyrev, and L. S. Wang, Angew. Chem. Int. Ed. 46, 4550 (2007).
- <sup>42</sup>C. Romanescu, T. R. Galeev, A. P. Sergeeva, W. L. Li, L. S. Wang, and A. I. Boldyrev, J. Organomet. Chem. 721-722, 148 (2012).
- <sup>43</sup>W. L. Li, A. S. Ivanov, J. Federič, C. Romanescu, I. Černušák, A. I. Boldyrev, and L. S. Wang, J. Chem. Phys. 139, 104312 (2013).
- <sup>44</sup>T. T. Chen, W. L. Li, H. Bai, W. J. Chen, X. R. Dong, J. Li, and L. S. Wang, J. Phys. Chem. A **123**, 5317 (2019).
- 45 W. J. Chen, M. Kulichenko, H. W. Choi, J. Cavanagh, D. F. Yuan,
   A. I. Boldyrev, and L. S. Wang, J. Phys. Chem. A 125, 6751 (2021).
- <sup>46</sup>W. J. Chen, Y. Y. Zhang, W. L. Li, H. W. Choi, J. Li, and L. S. Wang, Chem. Commun. 58, 3134 (2022).
- <sup>47</sup>T. T. Chen, L. F. Cheung, and L. S. Wang, Annu. Rev. Phys. Chem. **73**, 1 (2022).
   <sup>48</sup>H. J. Zhai, L. S. Wang, D. Yu. Zubarev, and A. I. Boldyrev, J. Phys. Chem. A **110**, 1689 (2006).
- <sup>49</sup>Q. Chen, H. J. Zhai, S. D. Li, and L. S. Wang, J. Chem. Phys. **138**, 084306 (2013).
- <sup>50</sup>Q. Chen, H. Bai, H. J. Zhai, S. D. Li, and L. S. Wang, J. Chem. Phys. 139, 044308 (2013).
- <sup>51</sup>L. Xie, W. L. Li, C. Romanescu, X. Huang, and L. S. Wang, J. Chem. Phys. 138, 034308 (2013).

- <sup>52</sup>W. L. Li, L. Xie, T. Jian, C. Romanescu, X. Huang, and L. S. Wang, Angew. Chem. Int. Ed. 53, 1288 (2014).
- <sup>53</sup>W. L. Li, T. T. Chen, D. H. Xing, X. Chen, J. Li, and L. S. Wang, Proc. Natl. Acad. Sci. U.S.A. 115, E6972 (2018).
- 54 T. T. Chen, W. L. Li, J. Li, and L. S. Wang, Chem. Sci. 10, 2534 (2019).
- 55 A. C. Reber and S. N. Khanna, J. Chem. Phys. 142, 054304 (2015).
- 56Y. J. Wang, L. Y. Feng, J. C. Guo, and H. J. Zhai, Chem. Asian J. 12, 2899 (2017).
- 57R. Yu, J. Barroso, M.-H. Wang, W.-Y. Liang, C. Chen, X. Zarate, M. Orozco-Ic, Z.-H. Cui, and G. Merino, Phys. Chem. Chem. Phys. 22, 12312 (2020)
- <sup>58</sup>H. Zhai, M. A. Ha, and A. N. Alexandrova, J. Chem. Theory Comput. **11**, 2385 (2015).
- <sup>59</sup>C. Adamo and V. Barone, J. Chem. Phys. **110**, 6158 (1999).
- 60 F. Weigend, Phys. Chem. Chem. Phys. 8, 1057 (2006).
- <sup>61</sup>T. H. Dunning, J. Chem. Phys. **90**, 1007 (1989).
- 62G. D. Purvis and R. J. Bartlett, J. Chem. Phys. 76, 1910 (1982).
- 63 M. J. Frisch et al., GAUSSIAN 16, Revision C.01, Gaussian, Inc., Wallingford, CT 2016
- **64**F. Neese, WIREs Comput. Mol. Sci. **2**, 73 (2012).
- <sup>65</sup>D. Y. Zubarev and A. I. Boldyrev, Phys. Chem. Chem. Phys. **10**, 5207 (2008).
- <sup>66</sup>A. I. Boldyrev and L. S. Wang, Phys. Chem. Chem. Phys. **18**, 11589 (2016).
- <sup>67</sup>M. Kulichenko, W. J. Chen, Y. Y. Zhang, C. Q. Xu, J. Li, and L. S. Wang, J. Phys. Chem. A 125, 4606 (2021).
- <sup>68</sup>M. Kulichenko, N. Fedik, K. V. Bozhenko, and A. I. Boldyrev, J. Phys. Chem. B **123**, 4065 (2019).
- <sup>69</sup>N. Fedik, M. Kulichenko, D. Steglenko, and A. I. Boldyrev, Chem. Commun. 56, 2711 (2020).
- <sup>70</sup>M. Kulichenko and A. I. Boldyrev, J. Phys. Chem. C 124, 6267 (2020).
- 71 P. Pyykkö, J. Phys. Chem. A 119, 2326 (2015).
- <sup>72</sup>W. L. Li, C. Romanescu, T. Jian, and L. S. Wang, J. Am. Chem. Soc. 134, 13228 (2012).
- <sup>73</sup>H. J. Zhai, Q. Chen, H. Bai, H. G. Lu, W. L. Li, S. D. Li, and L. S. Wang, J. Chem. Phys. **139**, 174301 (2013).
- $^{74}\mathrm{See}$  the supplementary material at <a href="https://www.scitation.org/doi/suppl/10.1116/6.0001833">https://www.scitation.org/doi/suppl/10.1116/6.0001833</a> for the molecular orbital analysis of the global minimum of Cu<sub>2</sub>B<sub>8</sub>, the AdNDP bonding analysis for the global minimum of neutral Cu<sub>2</sub>B<sub>8</sub>, comparison of the experimental data with TD-DFT calculations, and the Cartesian coordinates of the global minima and low-lying isomers of Cu<sub>2</sub>B<sub>8</sub> and Cu<sub>2</sub>B<sub>8</sub>.